Eur. Phys. J. Appl. Phys. (2012) 57: 21004
DOI: 10.1051/epjap/2011110392

THE EUROPEAN PHYSICAL JOURNAL APPLIED PHYSICS

Regular Article

Three-dimensional atomic magnetometry

H.F. Dong[a], J.C. Fang, B.Q. Zhou, X.B. Tang, and J. Qin

School of Instrumentation Science and Opto-Electronics Engineering, Beihang University, Science and Technology on Inertial Laboratory, Fundamental Science on Novel Inertial Instrument and Navigation System Technology Laboratory, 37#, Xueyuan Road, Beijing 100191, P.R. China

Received: 5 October 2011 / Received in final form: 1 December 2011 / Accepted: 5 December 2011
Published online: 30 January 2012 –

Abstract. Three-dimensional atomic magnetometry scheme is proposed and experimented. The scheme uses only one laser beam and can measure three components of the magnetic field independently. Spin-exchange-relaxation-free regime is verified by magnetic resonance measurement. The open loop scale factors of −2.722 mV/nT, −1.452 mV/nT and 0.076 mV/nT for the three axes are characterized. The model considering the frequency response and linewidth variation can fit the measurement data well. As only one laser beam is required, the magnetometry is easy to be realized on chip scale and is particularly attractive for applications requiring low power, low cost and high precision at the same time.

1 Introduction

There are two kinds of atomic magnetometry according to the measurement mechanism. One is transient atomic magnetometry which gets the scalar magnetic field information by measuring the Larmor procession frequency. Usually a small RF signal is locked to the Larmor frequency through lock-in and voltage-controlled oscillator system [1]. The other is steady-state atomic magnetometry which surveys the magnetic field by measuring the polarization vector after the procession. Orthogonal double-laser-beam scheme was proposed in 2002 to test the magnetic field perpendicular to both the pumping beam and the probe beam [2]. When the magnetic field is much smaller than the equivalent magnetic field of total relaxation rate, the output of the probe beam is linear with the magnetic field vector perpendicular to the light beams and the cross-sensitivity can be neglected. Furthermore, spin-exchange-relaxation-free (SERF) regime is realized which helps to improve the sensitivity of atomic magnetometer to the level of superconducting quantum interference device (SQUID) magnetometer [2]. This kind of atomic magnetometer has presently overpassed SQUID magnetometer and holds the record for magnetic field sensitivity of any device [3]. As atomic magnetometer has no requirement for cryogenic equipment, it has the potential to be fabricated on chip scale and the application range can be expanded greatly [4].

Unfortunately, the above double-laser-beam scheme has difficulties in the chip scale realization because it is difficult to fabricate the optical windows on the side of the microfabricated vapor cell. The inclined orthogonal double-beam scheme was realized using a dual chamber microfabricated cell in 2010 [5], in which the pumping and probe beams inclined from the plane of the chip. Besides the complexity of the double-beam structure, the inclination scheme makes it difficult to integrate the semiconductor laser and photodetector on a wafer level. By measuring the zero-field magnetic resonance of a single circularly polarized light propagating in a direction perpendicular to the static magnetic field B_0, single-laser-beam scheme has been demonstrated [6,7].

For many applications three-dimensional magnetometry is inevitable or preferred [8,9]. Seltzer and Romalis realize a three-dimensional vector atomic magnetometer with K vapor using orthogonal double-laser-beam scheme and cross-feedback system [10]. In this paper, we demonstrate a three-dimensional atomic magnetometry scheme with Cs vapor, which differs from the magnetometer proposed by Seltzer and Romalis [10] in that it uses only one laser beam. Compared with the research in [6,7], all the three-dimensional magnetic fields are measured, and the different models of the magnetometer are analyzed in detail. To achieve this, individual coils are installed around the vapor cell in an orthogonal configuration and the modulation fields are induced through coils in x-, y- and z-directions. The magnetic fields are demodulated individually by three lock-in amplifiers. The open loop characteristics of the magnetometer are measured in x-, y- and z-axes, respectively. The zero intercept of the open loop input/output relation means not only that the magnetometer can work at zero fields by feedback but

[a] e-mail: shanzhishan@gmail.com

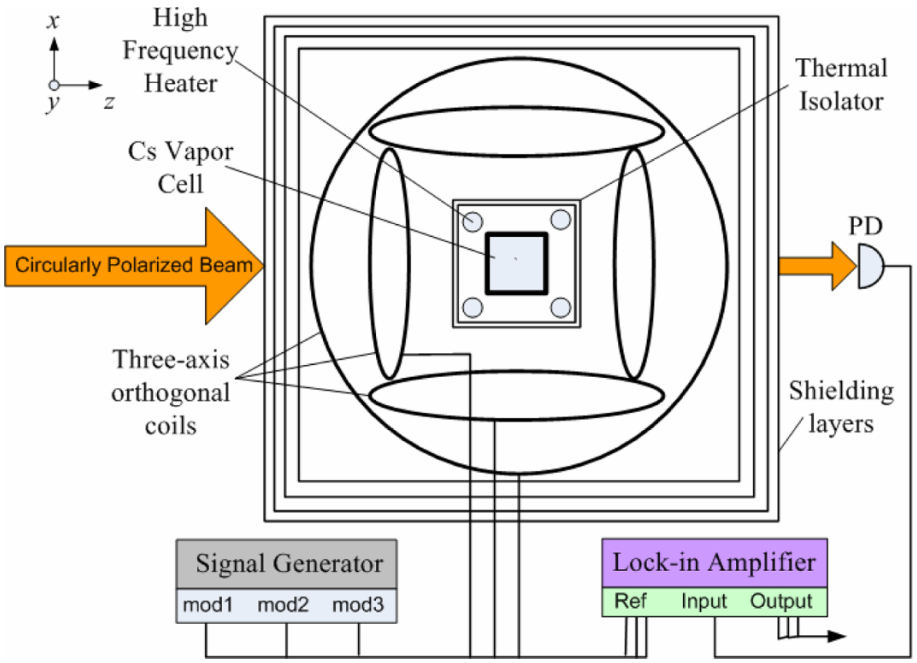

Fig. 1. (Color online) Setup of the three-dimensional atomic magnetometry.

also that the calibration during the application is simplified. The SERF regime is observed through comparing the measured linewidth with the theoretical linewidth. A similar demodulation method has been used in ^{4}He-pumped magnetometer, where the modulation frequencies are 9 Hz, 16 Hz and 20 Hz, and the modulation amplitude is 10^{-3} B (B is the measured magnetic field) [11]. In the experiments of this paper, we use much higher frequency (up to 210 Hz) and modulation amplitude (∼50 nT), which is close to the magnetic field range. Four models are investigated among which the subtractive model with the frequency response and the linewidth variation fits the experimental data very well.

2 Setup and magnetic resonance measurement of the magnetometer

The measurement setup is illustrated in Figure 1. The vapor cell containing Cs atoms, one amagat of buffer gas and 30 Torr of N_2 for quenching, is heated to 90–120 °C by four heaters with a high-frequency current of 100 mA at 30 kHz. The cell is a cylinder of ∅20 × 30 mm. The test is done in a four-layer magnetic shield together with the compensation of the residual magnetic field by the coils inside the shield. The magnetic modulation and compensation use the same coils. The zero-field magnetic resonances of different temperatures are measured using a circularly polarized laser tuned to D1 resonance at 894 nm. The absorption of the light is detected by a photodetector (PD). The light power is adjusted to 18.3 mW at 120 °C. The magnetic resonance at 120 °C, shown in Figure 2, has a full-width at half-maximum (FWHM) of

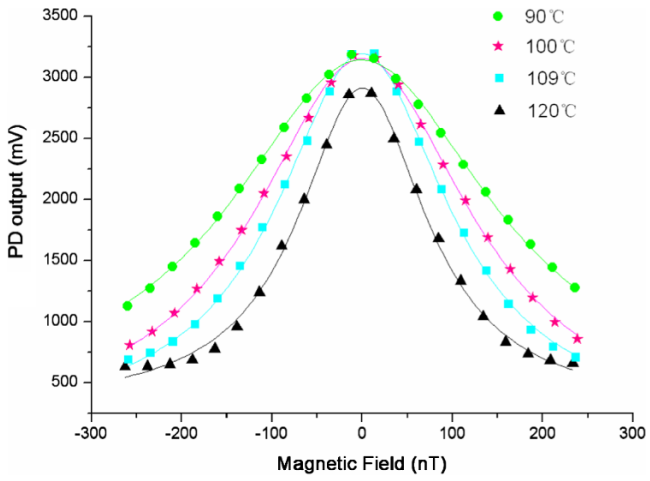

Fig. 2. (Color online) The magnetic resonance of the magnetometer. (The solid line is Lorentzian fit with full-width at half-maximum of 172 nT at 120 °C.)

172 nT. The linewidth obtained by extrapolating to zero light intensity is even smaller. By comparison, the estimated spin-exchange-limited linewidth at this temperature is 1832 nT which is higher by more than one order. This indicates that the magnetometer is operating in the SERF regime. For the measured linewidth of 172 nT, the contribution due to spin destruction is 17 nT, the other contributions to the linewidth include the diffusion and the light pumping.

As the linewidth is decided by the sum of light pumping rate, spin destruction relaxation rate and diffusion rate, etc., the real pumping rate can be obtained from the

measured linewidth, the theoretical calculation of spin destruction rate ($R_{sd} = n(T)v(T)\sigma_{sd} \approx 235\,\mathrm{s}^{-1}$ at 120 °C) and the diffusion relaxation rate estimated by the freely decaying fundamental diffusion mode [2] ($R_d \approx 124\,\mathrm{s}^{-1}$ at 120 °C). In this way the pumping rate is deduced to be about 480 s^{-1} and the corresponding polarization about 0.57. The values are smaller than those calculated directly from the pumping light power [12] ($R_p \approx 1953\,\mathrm{s}^{-1}$ at resonance, corresponding to a polarization of 0.85). The pressure of N_2 quenching gas in the vapor cell is 30 Torr, which is not high enough for eliminating the radiation trapping completely [13], so the radiation trapping is one reason for the reduction and the other reason is that the laser is operated under free running mode and the detuning can also reduce the pumping rate.

The fundamental sensitivity limit of atomic magnetometer is decided by [2]

$$\delta B = \frac{1}{\gamma\sqrt{nT_2Vt}}, \tag{1}$$

where γ is the gyromagnetic ratio in Hz/T, n is the density of atoms in m^{-3}, T_2 is the transverse spin relaxation time in second, V is the cell volume in m^3 and t is the measurement time in second.

The lower limit of T_2 can be deduced from the linewidth of the magnetic resonance illustrated in Figure 2 and the corresponding sensitivity is about 112 $\mathrm{fT}/\sqrt{\mathrm{Hz}}$ at 120 °C.

3 Three-dimensional open loop characterization of the magnetometer

To measure the three-dimensional vector magnetic fields separately, three modulation signals of different frequency are added to the three orthogonal coils, respectively (shown in Fig. 1). The signal of PD is input to a lock-in amplifier, in which the modulation signals of x, y and z coils are used as the reference. When the environment magnetic field keeps constant, the output of the photodetector will vary with the modulation field generated by the coil. The amplitude of the variation is decided by the environment field and the absorption line shown in Figure 2, which is then demodulated by the lock-in amplifier. The open loop input/output relation measurements are performed by sweeping the bias current of the coils around zero magnetic fields. The results are shown in Figure 3. The detailed comparison of different fitting models is shown in Figure 4. The open loop scale factors at zero field are −2.722 mV/nT, −1.452 mV/nT and 0.076 mV/nT for x-, y- and z-axes, respectively. Corresponding to the zero-field inputs, the outputs of x-, y- and z-axes are all zero, which means that under close loop mode the atoms may experience no or very small bias magnetic field and the system has no offset output. So the calibration for the application can be simplified [8]. The reason for the sign and value difference of the open loop scale factors of the three dimensions is explained as below.

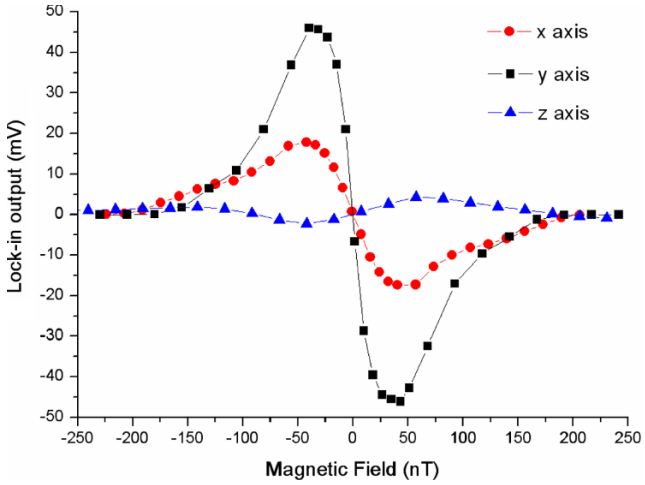

Fig. 3. (Color online) The three-dimensional open loop input/output relation of the atomic magnetometer.

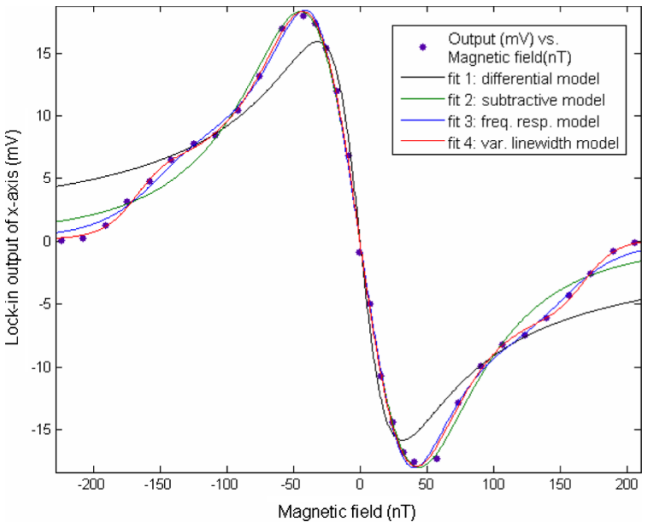

Fig. 4. (Color online) Different fitting models of the open loop input/output relation.

When there is polarization, the propagation of the light through the cell is governed by the amount of polarization [12],

$$\frac{\mathrm{d}R_p}{\mathrm{d}x} = -n\,(1 - P_z)\,\sigma(v)R_p, \tag{2}$$

where R_p is the pumping rate in s^{-1}, n is the density of the vapor in m^{-3}, P_z is the polarization along the pump beam with no dimension and $\sigma(v)$ is the absorption cross-section in m^2.

Assuming that the polarization along the pump beam through the cell is constant, and considering that the pumping rate is linear to the light power, we can get the output of the PD by solving equation (2),

$$PD_{\mathrm{output}} = PD_0 e^{-OD(1-P_z)}, \tag{3}$$

where PD_0 is the original output in watts or voltage, i.e., output of PD without any vapor absorption, OD is the

optical depth with no dimension, $OD = n\sigma(v)l$, where l is the length of light propagating through the vapor in m.

As OD is usually much smaller than 1 and $0 \leq P_z \leq 1$, equation (3) can be linearized by connecting the point of $P_z = 0$ and $P_z = 1$:

$$PD_{\text{output}} \approx PD_0(1-e^{-OD}) \times P_z + C_0 = k \times P_z + C_0, \quad (4)$$

where C_0 is the output of PD when $P_z = 0$, $C_0 = PD_0 \times e^{-OD}$ and P_z is the polarization of the vapor along the beam.

In the SERF regime, the dynamics of the atomic polarization can be well described by the Bloch equation [2,14]. Accordingly, polarization of the vapor along the beam can be calculated as

$$P_z = P_0 \frac{B_z^2 + (R_{\text{tot}}/\gamma)^2}{B_x^2 + B_y^2 + B_z^2 + (R_{\text{tot}}/\gamma)^2}, \quad (5)$$

where P_0 is the equilibrium polarization along the pump beam direction with no dimension, B_x, B_y and B_z are the vectors of the magnetic field in T, R_{tot} is the sum of pumping rate and relaxation rate in s^{-1} and γ is the gyromagnetic ratio in Hz/T.

The difference of the sign and value of scale factors for x, y and z fields can be explained basically by the differential model of the scheme. (The other models and their comparison are described in Sect. 4.) In this model, the outputs of the lock-in system are proportional to the derivative of PD output along the beam with respect to B_x, B_y and B_z, as shown in equations (6)

$$\begin{aligned}
\frac{\mathrm{d}PD_{\text{output}}}{\mathrm{d}B_x} &\approx -2PD_0(1-e^{-OD})P_0 \\
&\quad \times \frac{B_z^2 + B_{\text{equi}}^2}{(B_x^2 + B_y^2 + B_z^2 + B_{\text{equi}}^2)^2} B_x, \\
\frac{\mathrm{d}PD_{\text{output}}}{\mathrm{d}B_y} &\approx -2PD_0(1-e^{-OD})P_0 \\
&\quad \times \frac{B_z^2 + B_{\text{equi}}^2}{(B_x^2 + B_y^2 + B_z^2 + B_{\text{equi}}^2)^2} B_y, \\
\frac{\mathrm{d}PD_{\text{output}}}{\mathrm{d}B_z} &\approx 2PD_0(1-e^{-OD})P_0 \\
&\quad \times \frac{B_x^2 + B_y^2}{(B_x^2 + B_y^2 + B_z^2 + B_{\text{equi}}^2)^2} B_z, \quad (6)
\end{aligned}$$

where $B_{\text{equi}} = R_{\text{tot}}/\gamma$ in T.

From equations (6), we can see that the output is proportional to the original output PD_0, $1 - e^{-OD}$ and P_0. Theoretically, if these three parameters are equal, the scale factors of x- and y-directions must be equal. In the experiment, the temperatures are 100 °C and 103 °C for x- and y-axes, respectively. When the temperature increases, the absorption is increased and the signal is decreased. So during the experiment once the temperature increases, the light power is adjusted to balance the absorption. To reduce the adjustment times, we usually increase the light power until the original output of PD_0 reaches a higher value. The original output of PD_0 is 1.33 V and 1.79 V for x- and y-axes, respectively. Accordingly, the scale factor ratio of x- and y-axes is calculated to be 1.625, which is close to the measured data of 1.875. The reason why scale factor of z-axis is positive and those of x and y are negative can also be explained by equations (6). As we do the experiment in the magnetic shield, it can be seen from equations (6) that the scale factor of z-axis is small because both B_x and B_y are shielded. In the experimental setup, the x and y fields are shielded down to 1 nT, the theoretical scale factor along the pump beam is about 10^{-4} of that along the orthogonal direction. The measured data are about one-twentieth of the x-axis and one-fortieth of the y-axis. The reasons for this huge difference may be due to the residual magnetic field caused by high-frequency heating current of 100 mA at 30 kHz, and the modulation magnetic fields (∼50 nT) can lead to the same effect.

4 Modeling of the input/output relation of the magnetometer

In this section, we compare four models using the x-axis response as an example. When the modulation amplitude is small, the x-axis output of the lock-in amplifier can be obtained by equation (7)

$$\begin{aligned}
LI_{\text{dif.}} &\approx 2A_m \frac{\mathrm{d}PD_{\text{output}}}{\mathrm{d}B_x} \\
&= -4k' \frac{B_z^2 + B_{\text{equi}}^2}{\left(B_x^2 + B_y^2 + B_z^2 + B_{\text{equi}}^2\right)^2} A_m B_x, \quad (7)
\end{aligned}$$

where $k' = PD_0(1 - e^{-OD})P_0$ and A_m is the amplitude of the modulation field in T.

From equation (7), we know that the output of the lock-in amplifier is linear to B_x when B_x, B_y and B_z are much smaller than B_{equi}.

To increase the open loop scale factor of the magnetometer, we use large modulation amplitude, i.e., A_m in equation (7), up to 600 mV (corresponding to 50 nT). In this case the subtractive model, i.e., equation (8), fits the measurement results better, as shown by comparing fit 2 with fit 1 of Figure 4:

$$\begin{aligned}
LI_{\text{sub.}} = -k' \Bigg(& \frac{B_z^2 + B_{\text{equi}}^2}{(B_x + A_m)^2 + B'^2} \\
& - \frac{B_z^2 + B_{\text{equi}}^2}{(B_x - A_m)^2 + B'^2} \Bigg) B_x, \quad (8)
\end{aligned}$$

where $B' = B_y^2 + B_z^2 + B_{\text{equi}}^2$.

Furthermore, to help achieve the maximum linewidth of the magnetometer, the modulation frequency also needs to be increased. The data in Figure 4 are measured with a modulation frequency up to 210 Hz, and then the variation of the alternating response scale factor to the magnetic field must be considered in the model [14]. Because the resonant output happens at $\pm B_{\text{mod}}$ and the relation

Table 1. The comparison of pump-probe scheme and the single-pump scheme.

		Pump-probe scheme		Single-pump scheme
		Faraday modulator (FM)	Polarizing beam splitter (PBS)	Magnetic modulator (MM)
Output		I_{mod}	$I_1 - I_2$	I_{mod}
Noises	Laser amplitude noise	Small (limited by lock-in amplifier)	Small (common-mode noise is eliminated)	Small (limited by lock-in amplifier)
	Photodetector noise	Small (limited by lock-in amplifier)	Medium (limited by PD noise)	Small (limited by lock-in amplifier)
	Electromagnetic noise	Ignorable	Ignorable	Medium (limited by Johnson noise and current instability)
Scale factor around zero field		$\frac{I_{pr}R_p\gamma ncr_e fD(v)l\alpha}{R_{\mathrm{tot}}^2}$	$\frac{I_{pr}R_p\gamma ncr_e fD(v)l}{R_{\mathrm{tot}}^2}$	$\frac{4I_{\mathrm{pu}}R_p\gamma^2(1-e^{-ncr_e fL_{D1}(v)l})A_m}{R_{\mathrm{tot}}^3}$
Scale factor stability	Temperature	n is affected by temperature	n is affected by temperature	OD is affected by temperature
	Laser amplitude	I_{pr} is linear to the scale factor and R_p is also affected by I_0	I_{pr} is linear to the scale factor and R_p is also affected by I_0	I_{pu} is linear to the scale factor and R_p is also affected by I_0
Bias		Non-orthogonal angle	45° offset	Magnetic offset

Note: The scale factors of pump-probe scheme with FM and PBS are obtained from equations (2.101) and (2.106) in reference [16] and equation (2.62) in reference [12], while that of pump-probe scheme uses the differential model, i.e., equation (7) in this paper. The meaning of the parameters in Table 1 is as given below:
I_{mod} is the Fourier component of the detected light intensity at frequency w_{mod}. For FM, w_{mod} is the Faraday modulation frequency, and for MM, w_{mod} is the magnetic modulation frequency.
I_1 and I_2 are the light intensities of two separate beams (the polarizing beamsplitter is set at 45° to the initial polarization direction of the beam).
I_{pr} is the probe light intensity transmitted through the cell.
I_{pu} is the pump light intensity transmitted through the cell without any absorption, corresponding to PD_0 in equation (3).
R_p is the pumping rate.
γ is the gyromagnetic ratio.
n is atomic vapor density.
c is the light speed.
r_e is the radius of electron.
f is the oscillator strength of D1.
l is the length of interaction between atoms and light.
$D(v) = -D_{D1}(v) + D_{D2}(v)$ is the sum of dispersion line at D1 and D2 resonance.
α is the modulation angle of the Faraday modulator $L_{D1}(v)$ is the absorption line at D1 resonance.

between the magnetic field and output can be well described by a Lorentz line, the coefficient of correction in the model considering frequency response uses the sum of two symmetry Lorentz expressions, as shown in equation (9). The fitted curve of equation (9) is shown by fit 3 of Figure 4:

$$LI_{\mathrm{freq.resp.}} = \left(\frac{B_{lw}^2}{(B_x - B_{\mathrm{mod}})^2 + B_{lw}^2} + \frac{B_{lw}^2}{(B_x + B_{\mathrm{mod}})^2 + B_{lw}^2}\right) LI_{\mathrm{sub.}}, \quad (9)$$

where B_{mod} is the magnetic field corresponding to the modulation frequency in T, $B_{\mathrm{mod}} = w/\gamma$, w is the modulation frequency in Hz and B_{lw} is the magnetic linewidth in T.

In equation (9), B_{lw} is treated as a constant, however, as the magnetic fields increase, the resonance linewidth also increases due to the second-order contribution of spin exchange. Theoretically, for small atomic polarizations, relaxation due to spin exchange is quadratic in the magnetic fields, which vanishes for zero magnetic fields, as shown in equation (10) [15]:

$$R_{se}^{SERF} = \frac{(B \times \gamma/q)^2}{\sqrt{R_{se}}} \times \frac{q^2 - (2I+1)^2}{2}, \quad (10)$$

where R_{se} is the spin-exchange rate in s^{-1}, I is the nuclear spin and q is the slowing down factor with no dimension.

We compare the quadratic linewidth variation model with the linear linewidth variation model and find no distinctive difference. The reason may be that for the low

Table 2. The advantage and disadvantage of pump-probe scheme and single-pump scheme.

	Pump-probe scheme	Single-pump scheme
Advantage	• Higher scale factor • All-optical structure with no Johnson noise and current noise	• Single-laser beam • Easy to set up a close-loop system to expand the measurement range
Disadvantage	• Two laser beam • Narrow measurement range	• Johnson noise and current noise by oils

magnetic fields, the main contribution to the relaxation is due to the spin destruction, while for the higher magnetic fields, the quadratic model can be linearized with enough precision. So the linear linewidth variation model is used in equation (11). The fitted curve is shown by fit 4 of Figure 4. The adjusted coefficients of determination R^2 of equations (7)–(9) and (11) are 0.941, 0.990, 0.996 and 0.998, respectively, which means that the model considering the linewidth variation fits the data best:

$$LI_{\text{var.lin.}} = \left(\frac{(a|B_x|+b)^2}{(B_x - B_{\text{mod}})^2 + (a|B_x|+b)^2} + \frac{(a|B_x|+b)^2}{(B_x + B_{\text{mod}})^2 + (a|B_x|+b)^2} \right) LI_{\text{sub.}}, \tag{11}$$

where $a|B_x|+b$ is the linewidth variation with the magnetic field B_x.

5 Discussions and conclusions

Table 1 lists the detailed output parameters of pump-probe scheme using Faraday/photoelastic modulator and polarizing beam splitter, and single-beam scheme using a magnetic modulator. Given that the light intensity is the same, i.e., $I_{\text{pr}} = I_{\text{pu}}$, and $A_m = R_{\text{tot}}/\gamma_e$, under the same temperature, the maximum scale factor of pump-probe beam using PBS is larger by a factor of about 6 than that of single-pump scheme. Otherwise, the pump-probe scheme is an all-optical scheme so that there are no Johnson noise and current instability effects. The disadvantage of pump-probe scheme is that two beams are necessary and the measurement range is usually narrow. The advantage and disadvantage of these two schemes are summarized in Table 2.

In conclusion, a single-beam three-axis SERF magnetometer capable of independently measuring the three components of magnetic field has been described. The SERF regime is verified by comparing the measured linewidth with the theoretical linewidth caused by spin exchange. The open loop input/output relations for the three axes are characterized. Among the four different models compared, the subtractive model with the frequency response and the linewidth variation can fit the measurement data well even when the modulation amplitude is large and the modulation frequency is high.

The authors thank the support by National Natural Science Foundation of China under Grant Nos. 60736025, 61074171, 61121003 and Beijing Natural Science Foundation under Grant No. 3122025. The corresponding author would also like to thank Dr. M. Kashif Siddiq and Dr. Fenzhuo Guo for their careful proofreading and suggestions.

References

1. S. Groeger, G. Bison, J.-L. Schenker, R. Wynands, A. Weis, Eur. Phys. J. D **38**, 239 (2006)
2. J.C. Allred, R.N. Lyman, T.W. Kornack, M.V. Romalis, Phys. Rev. Lett. **89**, 130801 (2002)
3. H.B. Dang, A.C. Maloof, M.V. Romalis, Appl. Phys. Lett. **97**, 151110 (2010)
4. H. Dong, J. Fang, B. Zhou, J. Qin, S. Wan, Microsys. Technol. **16**, 1683 (2010)
5. W.C. Griffith, S. Knappe, J. Kitching, Opt. Express **18**, 27167 (2010)
6. J. Dupont-Roc, S. Haroche, C. Cohen-Tannoudji, Phys. Lett. A **28**, 638 (1969)
7. V. Shah, S. Knappe, P.D.D. Schwindt, J. Kitching, Nat. Photonics **1**, 649 (2007)
8. A. Balogh, Space Sci. Rev. **152**, 23 (2010)
9. F. Goldenberg, in *Proceedings of IEEE/ION Position, Location and Navigation Symposium, New York, 2006*, p. 684
10. S.J. Seltzer, M.V. Romalis, Appl. Phys. Lett. **85**, 4804 (2004)
11. O. Gravrand, A. Khokhlov, J.L. Le Mouel, J.M. Leger, Earth Planets Space **53**, 949 (2001)
12. T.W. Kornack, A test of CPT and Lorentz symmetry using K-3He co-magnetometer, Ph.D. thesis, Department of Physics, Princeton University, 2005
13. M.A. Rosenberry, J.P. Reyes, D. Tupa, T.J. Gay, Phys. Rev. A **75**, 023401 (2007)
14. M.P. Ledbetter, I.M. Savukov, V.M. Acosta, D. Budker, Phys. Rev. A **77**, 033408 (2008)
15. W. Happer, A.C. Tam, Phys. Rev. A **16**, 1877 (1977)
16. S.J. Seltzer, Developments in alkali-metal atomic magnetometry, Ph.D. thesis, Department of Physics, Princeton University, 2008